Title
On-demand droplet loading for automated organic chemistry on digital microfluidics

Journal
Lab on a Chip, 13(14)

ISSN
1473-0197

Authors
Shah, Gaurav J
Ding, Huijiang
Sadeghi, Saman
et al.

Publication Date
2013

DOI
10.1039/c3lc41363b

Peer reviewed

ON-DEMAND DROPLET LOADING FOR AUTOMATED ORGANIC CHEMISTRY ON DIGITAL MICROFLUIDICS

Gaurav J. Shah[1,2,5], Huijiang Ding[1,2], Saman Sadeghi[1,2], Supin Chen[3], Chang-Jin "CJ" Kim[3,4], R. Michael van Dam[1,2,3]

[1]Crump Institute for Molecular Imaging, [2]Department of Molecular & Medical Pharmacology, [3]Department of Bioengineering, [4]Mechanical and Aerospace Engineering Department, University of California, Los Angeles (UCLA), USA, [5]Sofie Biosciences, Culver City, CA, USA

1. ABSTRACT

Organic chemistry applications on digital microfluidic devices often involve reagents that are volatile or sensitive and must be introduced to the chip immediately before use. We present a new technique for automated, on-demand loading of ~1 µL droplets from large (~1 mL), sealed off-chip reservoirs to a digital microfluidic chip in order to address this challenge. Unlike aqueous liquids which generally are non-wetting to the hydrophobic surface and must be actively drawn into the electrowetting-on-dielectric (EWOD) chip by electrode activation, organic liquids tend to be wetting and can spontaneously flood the chip, and hence require a retracting force for controlled liquid delivery. Using a combination of compressed inert gas and gravity to exert driving and retracting forces on the liquid, the simple loading technique enables precise loading of droplets of both wetting and non-wetting liquids in a reliable manner. A key feature from a practical point of view is that all of the wetted parts are inexpensive and potentially disposable, thus avoiding cross-contamination in chemical and biochemical applications. We provide a theoretical treatment of the underlying physics, discuss the effect of geometry and liquid properties on its performance, and show repeatable reagent loading using the technique. Its versatility is demonstrated with the loading of several aqueous and non-aqueous liquids on an EWOD digital microfluidic device.

2. INTRODUCTION

The manipulation of liquids in the form of individually controlled discrete ('digitized') droplets, referred to as digital microfluidics [1], has gained tremendous interest over the last decade. Manipulation (e.g. transport, merging, mixing, splitting) of droplets already dispensed onto the digital microfluidics chip is well established and most commonly performed using electrowetting-on-dielectric (EWOD) [2]. However the "world-to-chip" interface is a critical but frequently overlooked issue. On-demand droplet dispensing on EWOD from an on-chip reservoir has been demonstrated [2],[3], but on-chip reservoirs are limited in volume by device size, and not amenable to storing certain types of liquid where evaporation (e.g. volatile liquids), vapor cross-contamination or exposure to atmosphere (e.g. air- or moisture-sensitive reagents) are undesirable. Fabrication of sealed structures for on-chip storage and dispensing has been shown [4] and could be possibly adapted to EWOD to address these limitations, but such structures require complex fabrication and the deformable elements may have limited chemical compatibility. Storing reagents in sealed off-chip reservoirs such as inert glass vials, and delivering them to the chip on-demand would be preferred in many scenarios. A pneumatically driven system for continuous droplet-generation from an off-chip reservoir has been reported for aqueous solutions [5]. However, this approach cannot be adapted for on-demand delivery, particularly in the case of non-aqueous liquids that wet even the hydrophobic surfaces commonly used in EWOD [6]. Unlike aqueous fluids which require application of driving force to overcome the opposing capillary pressure upon reaching the chip, wetting fluids require the application of a retracting force to avoid spontaneous flooding of the chip.

Accurate loading can be achieved by a precisely controlled flow into the chip using a positive displacement device like a syringe pump [7]. However, each liquid inlet would require its own pump, making this approach difficult to scale up to multi-reagent loading. Also, storage of volatile and/or moisture sensitive reagents in standard sealed vials would be difficult to implement with this approach as they would need to be first drawn into the syringe before being delivered to the chip. A gas-driven actuation system, where actuation of each reagent is controlled by a gas valve, is an attractive approach, especially for a multi-reagent loading system. Using a common compressed gas and/or vacuum source obviates the need for active wetted components like valves and pumps, making the system amenable to a cheap, compact and disposable "cassette" based model.

3. THEORY

3.1.Loading droplets of non-aqueous liquids

Unlike continuous droplet generation, on-demand droplet generation requires a stopping/retracting force to halt the incoming flow for an arbitrary amount of time until the next droplet is desired. For aqueous liquids, this force is intrinsically provided by surface tension because of the hydrophobic (low surface energy) surfaces like Cytop® or Teflon® in the EWOD chip. But this is not the case for non-aqueous liquids, which wet even low energy surfaces. Fig. 1 illustrates this difference when ~20 µL of non-wetting aqueous and wetting non-aqueous liquids are pipetted through an inlet hole into the gap between two Cytop®-coated surfaces (to simulate the commonly used two-substrate EWOD configuration). For water (Fig. 1(a-b)), the contact angle (θ) on Cytop® is greater than 90^{o}, and as such the surface tension (white arrows) acts to push the liquid out of the gap. As a result, the water droplet does not enter the gap even under the weight of the droplet sitting above the hole. Additional active actuation (e.g. EWOD) is needed to cause the liquid to enter the chip. On the other hand, for dimethyl sulfoxide (DMSO) (Fig. 1(c,d)), and other liquids having contact angle less than 90^{o}, such as acetonitrile (MeCN), the surface tension acts to pull the liquid into the gap (Fig. 1(c)). As a result, the liquid dispensed from the pipette immediately gets pulled into the gap (Fig. 1(d)). Activating EWOD electrodes only increases wetting further, so the amount of delivered liquid cannot be controlled from within the chip. Hence, while the surface tension forces can prevent a reservoir of an aqueous (non-wetting) liquid from flooding a hydrophobic coated device, a reservoir of a non-aqueous (wetting) liquid needs an external force to counteract the wetting forces and prevent it from flooding the microfluidic chip.

3.2.Pneumatic liquid loading against gravity

The challenge we seek to address is the "world-to-chip" interface for digital microfluidics, viz. how to interface the digital microfluidic chip, with volumes of a few microliters, with a reagent reservoir containing 100s of µL to several mL of liquid. A common form in which reagents are stored in chemistry labs is sealed, septum capped vials to prevent exposure to moisture and/or air, and/or to prevent evaporation, to ensure a long shelf life. At the time of use, the septa are pierced with a sharp tubing or needle and the reagents extracted from it. Such a format is also ideal for distributing "kits" with pre-measured amounts of various reagents needed for an assay or reaction. Our objective is to controllably deliver microfluidic volumes (1-20µL) of fluid from these larger reservoirs. Syringe pumps with chemically compatible syringes as a reservoir provides means to control force in both directions (i.e., driving and retracting), but this approach becomes cumbersome to expand to multi-reagent loading as every additional reagent requires an additional syringe pump, which adds to the overall cost and size. Pneumatically-driven transfer of liquids is easier to scale up for delivery from multiple reagent reservoirs as the active components (i.e. the pneumatic valves and pressure source) are not directly exposed to the liquid, thus avoiding contamination, corrosion, etc. However, the challenge is that the inherent compressibility of the gas leads to a long lag time for pneumatically driven liquid actuation, making it

harder to precisely control the volume of liquid pumped. This is particularly true for the case of wetting organic liquids, which tend to spontaneously flood into the chip.

Although negative pressure (vacuum) can be applied to the reservoir vial to pull back the liquid, the finite rate of gas removal from the line between the vacuum source and the reservoir vial leads to a delayed response. To enable on-demand μL-droplet loading from a 1.5mL off-chip reservoir vial without flooding the chip, we admit the fluid from the bottom of the chip such that the weight of a column of liquid (gravity) can serve as the counteracting force (Fig. 2(a,b)). Gravitational force provides a pullback force acting directly on the liquid being dispensed. Using a pneumatic driving force component that can be dynamically adjusted allows small, rapid pressure changes to switch between a net upward force and a net downward force on the vertical liquid column. This configuration permits sufficient control of the leading meniscus to enable on-demand droplet delivery.

Fig. 2(c,d) shows the main forces (ignoring viscosity) acting on a vertical column of liquid in a tube over a liquid reservoir. The EWOD chip is upside down compared with the traditional configuration. In the absence of applied pressure between the top and bottom of the tubing, the equilibrium between the surface tension (F_γ) and gravitational (F_g) forces determines the height of the liquid column, known as capillary rise (h_C), as given below.

$$F_\gamma = 2\gamma_{lv}\pi R_t \cos\theta_t \quad (1)$$

$$F_g = \pi R_t^2 h_{liq}\rho g \quad (2)$$

where R_t is the inner radius of the tubing, γ_{lv} is the liquid-vapor surface tension, θ_t is the contact angle of the liquid with the inside surface of the tubing, h_{liq} is the height of the liquid in the tubing, ρ is the liquid density and g is the gravitational acceleration.

At equilibrium, the capillary rise height h_c is:

$$h_c = \frac{2\gamma_{lv}\cos\theta_t}{\rho g R_t} \quad (3)$$

(Note: for θ_t>90°, h_c would be negative).

If the height of the liquid column (h_{liq}) exceeds h_c, the gravitational force will exceed the surface tension force, and provide a net downward force. Applying sufficient external pressure at the bottom of the tube would provide an upward force to raise h_{liq} beyond h_c so that the meniscus approaches the chip, but once the pressure is turned off, the net downward force described above will pull the meniscus away from the chip until the meniscus again sits at h_c.

By using a tubing of sufficient height ($h_t > h_c$), the capillary force alone is insufficient to draw the liquid into the chip. Therefore, the rise of the liquid out of the tube can be controlled by small changes in the applied pressure. For instance, using a tube with inner radius of of 0.3 mm, h_t>5cm would be sufficient to contain the capillary rise for various aqueous and non-aqueous liquids of interest. The theoretical capillary rise for some representative fluids is summarized in Table 1, with a conservative 'worst case' assumption of a fully wetting surface (θ_t=0°) and for the specific case of a Teflon tube using actual contact angles.

The required tube length can be reduced by increasing the inner diameter of the tube and using a hydrophobic surface coating on the inside of the tube to reduce wetting and hence $\cos\theta_t$. In fact, on a hydrophobic (e.g. Teflon®) surface, water would experience a negative h_c, since θ_t would be >90°.

Application of pressure force F_p with compressed gas applied into a closed (e.g. septum-capped) reservoir vial:

$$F_p = \pi R_t^2 p \quad (4)$$

can be used to overcome the gravitational force and actuate liquid up towards the chip (Fig. 2(e1-e2)). Neglecting contact angle saturation, viscosity, surface defects etc., the minimum pressure p_{min} required to generate enough force $F_{p,min}$, for the meniscus to reach the chip would be $p_{min}=\rho g(h_t - h_c)$.

Once (sufficient) liquid reaches the chip, the pressure is turned off (e.g. switching from pressure source to vent using a pneumatic valve) (Fig. 2(e3)), which causes gravity to again become the dominant force and provide the retracting force for the excess liquid (Fig. 2(e4)) that is not actively retained on the chip by EWOD force at the loading site. Thus, while maintaining the advantageous features of a purely pneumatic fluid pumping system (no wetted active components, easy multiplexing, no cross-contamination), the gravity pullback enables quick response times for on-demand loading without chip flooding.

It should be noted that the surface tension force is proportional to the radius of the advancing meniscus of the liquid column. Before reaching the chip, therefore, this force is constant and determined by the radius of the tubing (Fig. 2(c)), Eq. 1). We assume that when the liquid enters the chip it forms a circular meniscus on both substrates centered around the inlet hole with radius R_d. After entering the chip once the tubing is completely filled, F_γ is therefore proportional to the radius of the growing droplet inside the chip (Fig. 2(d)), Eq. 5):

$$F_\gamma = 4\pi R_d \gamma_{lv} \cos\theta \quad (5)$$

where θ is the contact angle of the droplet meniscus with the chip surface. Once the liquid reaches the chip surface having θ<90^o, the surface tension force inside the chip pulls liquid into the chip with a force that is directly proportional to the growing radius R_d, that will lead to flooding even in the absence of any other driving force such as pressure. The gravitational force F_g, which increases as the liquid rises in the column, becomes constant once the liquid enters the chip, given by the weight of the liquid in the filled column in the tube:

$$F_g = \pi R_t^2 h_t g \quad (6)$$

In the absence of pressure, as long as R_d is small enough that F_γ pulling liquid into the chip is less than F_g, droplet growth into the chip will decelerate, stop, and reverse.

If the velocity of the meniscus is too high, it will not be possible for F_g, even in the absence of applied pressure, to slow and reverse the droplet growth before a size of radius R_d has been reached, at which point flooding of the chip would begin. To reduce the possibility of runaway droplet growth, pressure driving the liquid upwards is applied in the form of pulses, such that the meniscus is nudged increasingly higher, each pulse followed by partial retraction of the meniscus by venting the pressure source. The application of pulsed pressure reduces the average meniscus speed and thus the likelihood of flooding. Another precaution is that the inlet hole is located close to the EWOD electrode at the loading site, so that liquid can be sensed, and the droplet can be split by EWOD before the droplet radius R_d grows too large and flooding ensues. The gravity-assisted microliter droplet creation using EWOD is discussed in the next section.

3.3.Gravity-assisted microliter-droplet creation

Using gravity as a retracting force can enable the on-demand introduction of discrete droplets of a wide range of liquids quickly into the chip without flooding. This section discusses the next step of micro-droplet creation (i.e., splitting from the liquid column) on chip, which is a critical capability for digital microfluidics [2].

For purely EWOD-based droplet creation from an *on-chip* reservoir, where EWOD actuation is applied at the 'reservoir' and the 'creation site' electrodes, a splitting criterion has been reported that establishes the conditions for the droplet completely separating from the reservoir [2],[3]. Based on droplet and electrode geometry (contact angle, electrode width, gap between substrates), the Laplace pressures at the 'separation' site (referred to in this paper as the 'necking' region) and the electrowetted extremities of the stretched droplet are determined. If there exists a net positive pressure difference between the necking site and the two extremities of the droplet when the neck width approaches zero, then there is a flow of liquid out of the necking site, leading to depletion and disappearance of fluid in the neck and thus leading to droplet splitting or creation. (Droplet creation is essentially an asymmetric case of droplet splitting.) Using contact angle values for water on Teflon® with no voltage applied (at necking site) and with EWOD voltage applied (at reservoir and creation site electrodes), a simple splitting criterion is obtained based the electrode width and gap between substrates [2]. It also follows that the greater the pressure difference between the necking region and electrowetted extremities, the greater the flow rate out of the necking site, and hence, the greater the tendency to split [3].

Using a theoretical treatment analogous to this approach, we can evaluate a splitting criteria for gravity assisted micro-droplet creation in our system where the on-chip reservoir has been replaced by an inlet hole (radius R_h) with vertical tubing below it leading to an off-chip reservoir vial below the device. Fig. 3 illustrates the geometry in gravity-driven droplet generation. EWOD voltage is applied on an electrode of width w_e located at a distance d_{he} from the hole. As discussed above, liquid is driven up into the chip through the vertical tubing (height h_t) between the reservoir vial and the EWOD chip at the inlet hole (radius R_h). Once liquid enters the chip and wets the actuated EWOD electrode, the driving pressure is eliminated (by venting the reservoir vial), allowing gravity to pull back the excess liquid. For a droplet to be left behind, it is important that the bulk fluid separates from the droplet held at the EWOD electrode.

We consider the case just before droplet splitting, such that the neck is extremely thin. In this scenario, if there is a positive pressure difference between the neck (n) and the electrode rightmost edge (e) as well as the neck and the hole (h), then liquid will continue to flow out of the neck leading to droplet creation (splitting). Similar to [3], the pressure at n and e are determined by the Laplace pressures, based on the radii of curvature r_n, R_n and r_e, R_e respectively. The Laplace pressure (above atmospheric pressure) at n and e can be determined geometrically:

$$p_n = \gamma_{lv}\left(\frac{1}{R_n} + \frac{1}{r_n}\right) \quad (7)$$

$$p_e = \gamma_{lv}\left(\frac{1}{R_e} + \frac{1}{r_e}\right) \quad (8)$$

As derived in [2], the pressure difference between the non-electrowetted n and the electrowetted e sites is given by:

$$p_n - p_e = \gamma_{lv}\left(\frac{1}{R_n} - \frac{1}{R_e} + \frac{\cos\theta_e - \cos\theta_n}{d_g}\right) \quad (9)$$

where ϑ_n and ϑ_e are the non-electrowetted and electrowetting-induced contact angles respectively, and d_g is the gap between the substrates of the EWOD chip. If we ignore contact angle hysteresis, the change in contact angle is proportional to the square of applied EWOD potential. The third term can be expressed in terms of the potential V_d across the dielectric layer (permittivity ε_{rd}, thickness d_d):

$$p_n - p_e = \gamma_{lv}\left(\frac{1}{R_n} - \frac{1}{R_e} + \frac{\varepsilon_0 \varepsilon_{rd} V_d^2}{2\gamma_{lv} d_g d_d}\right) \quad (9')$$

Since the vial is vented, the bottom of the liquid column is at atmospheric pressure and hence the gauge pressure at the inlet hole is given by:

$$p_h = -\rho g h_t \quad (10)$$

From Eqs. (7) and (10):

$$p_n - p_h = \gamma_{lv}(\frac{1}{R_n} - \frac{\cos\theta_n}{d_g}) + \rho g h_t \quad (11)$$

Analogous to [2], the droplet will be split from the liquid in the tubing if:

p_n-$p_e \geq 0$ and p_n-$p_h \geq 0$ (12)

Eq. (9), (11) and (12) form the splitting criteria for our system. We examine the effect of various geometrical and material parameters on the splitting criteria in the Results and Discussion section.

4. MATERIALS AND METHODS

4.1.EWOD device fabrication

The bottom substrate of the parallel-plate EWOD chip was fabricated from a 700 µm thick glass wafer coated with 140 nm indium tin oxide (ITO) (Semiconductor Solutions LLC, USA). The wafer was first covered with 20 nm of chromium and 200 nm of gold using an e-beam evaporator. Metal and ITO layers were etched to form EWOD electrodes (2.5 mm x 2.5 mm), connection lines, and contact pads. 1 µm silicon nitride was coated as a dielectric layer by plasma-enhanced chemical-vapor-deposition (PECVD), and 1 µm of Cytop® was spin-coated and annealed at 200°C to make the surface hydrophobic. A top substrate (cover plate) was prepared from 700 µm thick glass coated with 150 nm ITO (Delta Technologies Inc., USA) to serve as a ground electrode for electrowetting. The cover plate was coated with PECVD silicon nitride (100 nm) and Cytop® (100 nm). One edge of the cover plate was also coated with Cytop® film and served as the reagent-loading edge. The cover plate was affixed to the bottom EWOD substrate with double-sided adhesive (3M Inc., USA) such that the reagent-loading edge was aligned with the edge of the loading electrode on the bottom EWOD substrate. The nominal adhesive thickness (and thus gap height) was 100 µm.

4.2.Reagents

Acetonitrile, anhydrous dimethyl sulfoxide, methanol, potassium carbonate and hydrochloric acid were purchased from Sigma-Aldrich and used as received**.** Deionized **(**DI) water was generated in-house (Mettler Toledo Thornton, 200CRS).

4.3.Experimental setup and operation

Fig. 2(a) and Fig. 2(b) show a schematic and photograph of the experimental setup. A 1.5mL septum-capped vial serves as the off-chip reservoir, connected to the EWOD device above it via 20G needle (0.91mm OD, 0.61mm ID). The total length of the fluidic path between the vial and chip is ~7cm, and the internal surface is hydrophobic (Teflon® or Cytop®). A second needle is inserted in the vial to pressurize the headspace above the liquid and provide a pneumatic actuation force, F_p. This needle is connected to a compressed inert gas source via a pneumatic valve (not shown in Fig. 2(b)). The pneumatic force can be activated and deactivated such that the total resultant force on the liquid column can be toggled between upward and downward, respectively. F_p is designed to be sufficient to overcome the sum of the gravitational and surface tension forces and drive the meniscus all the way to the top of the tube. (For example, for water in a hydrophobic tubing, a pressure of at least ~0.83 kPa must be applied to barely overcome the downward acting gravity and surface tension force, ignoring contact angle hysteresis).

The steps of operation as described in Fig. 2(e) [6]. An electronically controlled pneumatic valve supplied with pressurized nitrogen is toggled on-demand to regulate pressure in the septum-capped reservoir vial, driving the liquid up the tube towards the device (Fig. 2(e1-e2)). In order to limit the momentum build-up and reduce the risk of flooding while maintaining quick response time, pressure is applied in a pulsed **(**~5

Hz, with ~50 ms pulse width, typically ~5-10 kPa amplitude) rather than constant fashion. The loading site has the EWOD electrode actuated with a potential of 100 V_{rms} (at 10kHz) to ensure that this area on the device is preferentially wetted by the incoming liquid. The same electrical signal is also used to electrically detect the impedance change in the loading site. Liquid enters the chip and fills up the loading site until the electrode in the loading site senses the transition in impedance from the "dry" (no liquid at loading site) to the "wet" (loading site filled above a threshold) state (Fig. 2(e3)) [7],[8]. Upon sensing the transition, the pressure is vented by toggling off the pneumatic valve. Under the right conditions (as discussed later in Section 5) a droplet is split off and held back on the chip at the electrowetted loading site, while the excess liquid is pulled back into the reservoir by gravity (Fig. 2(e4)).

A camera (DinoLite Digital Microscope) located vertically above the EWOD device was used to take images and monitor droplet loading. Droplet volume was estimated using image analysis (ImageJ) to measure the droplet footprint and multiplying it by the gap height.

4.4. Calculations for rising meniscus and splitting criteria

Plots for forces acting on the meniscus rising in the tubing and spreading from the inlet hole into the chip were made using a MATLAB simulation based on liquid properties from literature (Table 1) and geometrical properties of the device as described above. MATLAB simulations were also used to calculate the radius of curvature R_n for the splitting pressures calculation by solving the quadratic equation relating it to hole radius (R_h), hole-to-electrode distance (d_{he}) and electrode width (w_e) (See Fig. 3). Splitting pressures were then calculated using geometric parameters and material parameters for three fluids and plotted using MATLAB.

5. RESULTS AND DISCUSSION

5.1. On-demand loading without flooding

Using the system for pneumatic loading with gravitational pullback, we demonstrate the on-demand loading of organic and aqueous solvents. Fig. 4 shows the top view schematic (Fig. 4(a-d)) and image sequences (Fig. 4(e- l) for controlled, on-demand loading of two consecutive MeCN droplets from a large off-chip reservoir. Each of the droplet loading steps took under 5 s from the start of pumping to the formation of the discrete droplet loaded onto the chip.

Additional organic solvents (wetting liquids) such as DMSO (Fig. 5(b)) and MeOH (Fig. 5(c)) were similarly loaded onto the chip without flooding. While the technique enables flooding-free loading of organic solvents, it has the flexibility also to work with non-wetting liquids as demonstrated by loading water (Fig. 5(d)) and aqueous ionic solutions (e.g. 0.1N hydrochloric acid in water (Fig. 5(e)). Salt solutions and solutions containing mixtures of organic and aqueous solvents (e.g. 25mM potassium carbonate in 90:10 acetonitrile:water (Fig. 5(f)) were also loaded onto the chip using the same setup. Droplet sizes were measured using ImageJ and the results are summarized in Table 2. In each case, multiple droplets (≥5) were loaded and measured to have consistent volumes (standard deviation of ~5% or less for a given liquid). More wetting reagents tend to form droplets of larger volumes than the aqueous reagents for the geometrical parameters of the device and the setup used in these experiments, as discussed in Section 5.3.

5.2. Simulation of forces on rising meniscus

In this section, we present a simulation to help explain the mechanism and performance of the liquid loading technique. We first consider the case of liquid rising from the reservoir vial before it reaches the loading site. As discussed in the theory section, the forces acting in this case are F_g, F_γ and F_p. For a given inner radius of tubing, if h_t is chosen to be longer than the capillary rise h_c for all the liquids used, then F_g and F_γ would come to equilibrium at some point within the tubing in the absence of external pressure. When the reservoir vial is pressurized, the positive upward F_p would push the liquid towards the chip and if sufficiently high, all the way into the chip. For this discussion, we define "meniscus distance", x_m as the

distance of the farthest point of the advancing meniscus in the tubing or chip from the liquid in the reservoir vial:

$$x_m = \begin{cases} h_{liq} \text{ for } x_m \le h_t \text{ (i.e. in tubing)} \\ h_t + R_d \text{ for } x_m > h_t \text{ (i.e. in chip)} \end{cases} \quad (13)$$

Fig. 6 shows the results of simulated forces for three representative liquids: MeCN, DMSO and water using geometry and surface properties corresponding to experimental parameters. The individual force components F_g, F_γ and F_p, as discussed in the theory section, are shown along with the total force F_{tot}. The total force is calculated for two different pressures applied to the reservoir vial: 0 and 5 kPa.

In the absence of applied external pressure, the force on the liquid column is described by the solid red line in Fig. 6 (a,b,c). The forces would balance (F_{tot} = 0) when the meniscus was located at the capillary rise height h_c, and liquid would not reach the chip. (Note that in case of water, h_c is negative and not shown on the graph.) To drive the meniscus above h_c and into the chip, external pressure is applied (5 kPa depicted in the simulation). In this situation, the force on the liquid column is described the solid black line. F_{tot} is positive for all $x_m \le h_t$ in all three liquids, (although the magnitudes vary with liquid properties) indicating that, even with this low pressure, liquid in all three cases would accelerate into the chip from h_c. Conversely, turning off the pressure causes a return to the solid red line, where $F_{tot} < 0$ for $h_t > x_m > h_c$, pulling the liquid column down, away from the chip.

Inside the chip (i.e., $x_m > h_t$), F_γ is given by Eq. 5 and rises as the droplet radius R_d grows, while the downward gravitational force F_g remains constant as given by Eq. 6. For a wetting liquid like MeCN or DMSO (Fig. 6(a, b)), the increasing F_γ and constant F_g increase the tendency for liquid to enter and spread into the chip, as indicated by the rising positive force, leading to the 'runaway' or flooding phenomenon described earlier. But if the pressure is turned off (i.e., triggered when liquid is detected at the loading site), F_{tot} shifts from the black solid line to the red solid line where it is negative, and the meniscus decelerates and reverses direction, moving out of the chip due to the restoring effect of F_g. The case for a non-wetting liquid like water (Fig. 6(c)) is a bit different from the organic liquids as F_γ tends to push liquid out of the chip and therefore provides a force acting in the same direction as F_g to counteract the droplet spreading in the chip. The net force F_{tot} in this case goes to zero and then negative within a short distance in the chip even with applied pressure in the reservoir. Runaway flooding does not occur with non-wetting liquids. Thus, although gravity is not essential in the case of non-wetting liquids, the same droplet loading approach is compatible with both wetting and non-wetting liquids.

In summary, the counteracting force of gravity provides a rapid locally-acting pullback force that prevents uncontrolled flow of wetting fluids (e.g. organic solvents) into the chip and enables pneumatic pumping of microliter-scale volumes from much larger reservoirs. Unlike syringe pump-based approaches, sub-microliter control is hard to achieve with this technique. But in many practical applications where such accuracy is not needed, and/or where overall compactness and cost are more important considerations, this gas-driven approach becomes very attractive.

5.3. Splitting pressure: influence of liquid properties and geometry

We discussed above the controlled introduction of liquid into the chip and retraction of liquid from the chip. We next consider the critical step of droplet splitting, i.e. retaining a small amount of liquid while pulling back the rest of the liquid. As derived in the Theory section, droplet splitting will occur if the two splitting criteria (Eq. 12) are met. The two pressure differences p_n-p_e (Eq. 9) and p_n-p_h (Eq. 11) are dependent on various material and geometrical factors, which we consider here. For simplicity, we assume that the tubing is the same material as the chip surface (e.g., a fluoropolymer like Cytop® or Teflon®). We first consider the influence of the liquid properties, viz. density and surface tension, on the pressures p_n, p_h and p_e, and hence the splitting pressure differences, p_n-p_h and p_n-p_e.

The density of the liquid does not affect p_n and p_e, but from Eq. 10, higher density of the liquid increases the magnitude of (negative) p_h leading to a stronger gravitational pullback force and thus increasing p_n-p_h (Eq. 11). Increased liquid density therefore increases the tendency for outward flow from the necking region and therefore encourages splitting.

Next, we consider the effect of surface tension of the liquid, γ_{lv}. Increasing the surface tension increases the magnitude of p_n-p_e (Eq. 9, 9') but its direction is not immediately obvious. The third term of p_n-p_e in Eq. 9 is always positive since the electrowetted contact angle θ_e is always lower than θ_n and both are <180°. The sum of first two terms is negative, but for a wide range of dimensions typically used in EWOD devices and empirically observed contact angles from literature (at no applied potential [9] and at EWOD potential [10] for device geometry close to our conditions), the third term dominates. Thus, higher surface tension increases the splitting pressure, p_n-p_e. The other splitting pressure, p_n-p_h, also depends on γ_{lv} but only through p_n. From Eq. 11 and as discussed above, p_n contributes positively for non-wetting fluids and negatively for wetting fluids. Therefore increasing γ_{lv} for non-wetting fluids also increases the splitting pressure p_n-p_h, but reduces it for wetting fluids.

Fig. 7 shows a simulation of the variation of the splitting pressures with various geometric parameters for three representative liquids: two wetting (MeCN, DMSO) and one non-wetting (water) on hydrophobic Teflon® or Cytop® surface. The default conditions for the gap height, hole-to-electrode distance, electrode width and hole radius are, respectively:

d_g = 0.15mm; d_{he} =1.5 mm; w_e = 2.5 mm; R_h = 0.5 mm;

In general, it is evident from Fig. 7 that the splitting pressures p_n-p_h and p_n-p_e are stronger for water (red) than for MeCN (blue) and DMSO (green). This is to be expected (from Eq. 7) since p_n is positive for the non-wetting water (due to the positive cross-sectional curvature ($1/r_n$) which dominates over the negative in-plane curvature ($1/R_n$)) and negative for wetting liquids (since both the radii of curvature are negative). For wetting fluids, therefore, p_e and p_h need to be even more negative for the net splitting pressures to be positive. As a result, liquid would tend to flow quicker from the necking site for non-wetting liquids than wetting liquids. This may explain the observed differences in volume and shape of droplets created, with droplets of non-wetting fluids (Fig. 5d,e) being much more conformal to the electrode shape while those of wetting fluids (Fig. 5a,b,c,f) tend to be slightly larger than the electrode. That is, the size of the droplet formed seems to be inversely correlated to the surface tension of the liquid. This is consistent with the decreasing p_n-p_h with increasing surface tension for wetting fluids (see above in this section). Though outside the scope of the present work, we are investigating how geometric parameters such as hole-electrode distance, width of the electrode etc. to reduce the variations among different liquids in the dynamic necking process and thereby achieve a droplet size that is more consistent for different types of liquids.

It should be noted that the effect of dielectrophoretic (DEP) force due to the electric field present in the gap is not considered by the above criterion based on Laplace pressure change. Since most liquids would experience positive DEP force in an air-filled environment, this force would also help enhance the tendency of droplet splitting (by further lowering p_e), and its effect could be appreciable. But for simplicity, we have not considered its contribution to splitting.

We next consider the effect of various geometric parameters, viz. gap height, hole radius, hole to electrode distance and electrode width, of the chip on the two splitting criteria.

The effect of increasing gap height is to increase the magnitude of r_n (Fig. 3). For gap heights (d_g) that are small compared to the in-plane dimensions (i.e. R_n~1-3 mm), p_n is dominated by r_n term (Eq. 7). For non-wetting fluids (positive r_n), decrease in gap height thus increases the magnitude of p_n and therefore leads to an increase in splitting pressures, and for wetting fluids (negative r_n) it decreases the magnitude of p_n and leading to a decrease in splitting pressures. As gap height increases in relation to the in-plane dimensions, the dominance of r_n reduces, mitigating the influence of gap height on splitting pressure.

Other geometrical parameters on the chip include the hole radius (R_h), hole-to-electrode distance (d_{he}) and electrode width (w_e). These dimensions influence the in-plane radius of curvature at the necking site, R_n which is negative for both wetting and non-wetting liquids. A larger d_{he} decreases the magnitude of the negative in-plane curvature $1/R_n$ and hence increases p_n (Eq. 7), thus increasing the splitting pressures (Fig. 7(b)).

For increasing w_e, it turns out from geometry that the magnitude of $1/R_n$ decreases and hence p_n increases with increasing w_e, leading to a slightly higher splitting pressure for all other parameters held constant (Fig. 7(c)). The hole radius is also geometrically related to R_n (Fig. 3) but its effect is not significant in the dimensional range to the geometry used, as indicated by the nearly flat lines (Fig. 7(d)).

6. Conclusions

We have presented a versatile and robust technique for on-demand delivery of liquids to a digital microfluidic chip from an off-chip reservoir. The technique can be used for both aqueous and non-aqueous reagents, as is often needed in organic chemical synthesis. Liquid is pumped to the chip using pneumatic (pressure) force, while controlled droplet generation without chip flooding is performed using a combination of gravity and digital microfluidic actuation. The volume of droplets of a given liquid was found to be repeatable, falling with a standard deviation of <5% for several aqueous and organic liquids. The droplet volume differed for different liquids, but this could be compensated in various ways such as selection of loading electrode size if important for a particular application. A theoretical discussion of the forces involved, and the effect of geometric and material parameters on droplet generation is provided to support the experimental results for various aqueous and organic liquids. The specimen liquids used in this work span a wide range of properties, most importantly surface tension and density. Thus, we anticipate that the technique presented here can be extended to many other solvents and reagents used in organic chemistry, provided that they can be actuated using EWOD digital microfluidics [10].

Based on gas-driven fluidic flow, the technique does not require the use of liquid pumps and valves, allowing the use of compact, cheap and disposable wetted components (i.e., needles and vials) and easier expansion to a multiple reservoir system with minimum additional cost and size. The entire system is automated through software-controlled gas valve actuation, so as to reduce labor and as well as increase safety from chemical exposure. The automated remote operation becomes even more important for radiochemistry, e.g. for positron emission tomography (PET) probe production on digital microfluidics chips [11], in minimizing radiation exposure hazards.

7. Acknowledgments

This work was supported in part by the Department of Energy Office of Biological and Environmental Research (DE-SC0001249, DE-SC0005056) and the UCLA Foundation from a donation made by Ralph & Marjorie Crump for the UCLA Crump Institute for Molecular Imaging.

8. References

[1] R. Fair, “Digital microfluidics: is a true lab-on-a-chip possible?,” *Microfluidics and Nanofluidics*, vol. 3, no. 3, pp. 245–281, Jun. 2007.

[2] S. K. Cho, H. Moon, and C.-J. Kim, “Creating, transporting, cutting, and merging liquid droplets by electrowetting-based actuation for digital microfluidic circuits,” *J. MEMS*, vol. 12, no. 1, pp. 70–80, Feb. 2003.

[3] J. Gong and C.-J. Kim, “All-electronic droplet generation on-chip with real-time feedback control for EWOD digital microfluidics,” *Lab Chip*, vol. 8, no. 6, pp. 898–906, 2008.

[4] L. Xie, C. S. Premachandran, M. Chew, and S. C. Chong, “Development of a Disposable Bio-Microfluidic Package With Reagents Self-Contained Reservoirs and Micro-Valves for a DNA Lab-on-a-Chip (LOC) Application,” *IEEE transactions on advanced packaging*, vol. 32, no. 2, pp. 528–535, 2009.
[5] H. Ren, R. B. Fair, and M. G. Pollack, “Automated on-chip droplet dispensing with volume control by electro-wetting actuation and capacitance metering,” *Sensors and Actuators B: Chemical*, vol. 98, no. 2–3, pp. 319–327, Mar. 2004.
[6] G. J. Shah, H. Ding, S. Sadeghi, S. Chen, C.-J. Kim, and R. M. van Dam, “Milliliter-to-microliter platform for on-demand loading of aqueous and non-aqueous droplets to digital microfluidics,” in *Proceedings of the 16th International Solid-State Sensors, Actuators and Microsystems Conference (TRANSDUCERS)*, 2011, pp. 1260–1263.
[7] H. Ding, S. Sadeghi, G. J. Shah, S. Chen, P. Y. Keng, C. J. Kim, and M. van Dam, “Accurate dispensing of volatile reagents on demand for chemical reactions in EWOD chips,” *Lab on a Chip*, vol. 12, pp. 3331–3340, 2012.
[8] T. Thorsen, R. W. Roberts, F. H. Arnold, and S. R. Quake, “Dynamic Pattern Formation in a Vesicle-Generating Microfluidic Device,” *Phys. Rev. Lett.*, vol. 86, no. 18, p. 4163, Apr. 2001.
[9] W. M. Haynes, “CRC handbook of chemistry and physics,” 2010.
[10] D. Chatterjee, B. Hetayothin, A. R. Wheeler, D. J. King, and R. L. Garrell, “Droplet-based microfluidics with nonaqueous solvents and solutions,” *Lab Chip*, vol. 6, no. 2, pp. 199–206, 2006.
[11] S. Lee, J.-S. Park, and T. R. Lee, “The Wettability of Fluoropolymer Surfaces: Influence of Surface Dipoles,” *Langmuir*, vol. 24, no. 9, pp. 4817–4826, May 2008.
[12] S. Sadeghi, H. Ding, G. J. Shah, S. Chen, P. Y. Keng, C.-J. Kim, and R. M. van Dam, “On Chip Droplet Characterization: A Practical, High-Sensitivity Measurement of Droplet Impedance in Digital Microfluidics,” *Anal. Chem.*, vol. 84, no. 4, pp. 1915–1923, 2012.
[13] P. Y. Keng, S. Chen, H. Ding, S. Sadeghi, G. J. Shah, A. Dooraghi, M. E. Phelps, N. Satyamurthy, A. F. Chatziioannou, C.-J. Kim, and R. M. van Dam, “Micro-chemical synthesis of molecular probes on an electronic microfluidic device,” *PNAS*, vol. 109, no. 3, pp. 690–695, 2012.

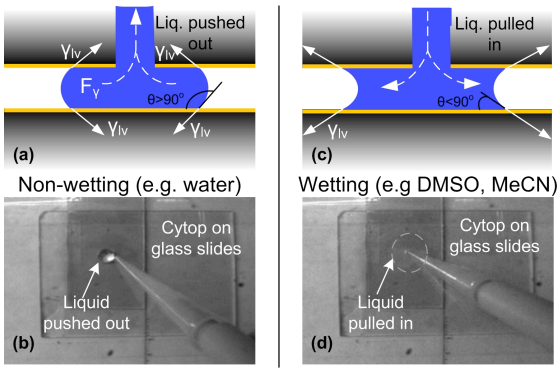

Fig. 1: Experiment demonstrating the different properties of aqueous and non-aqueous reagents showing why the latter cannot be stored in reservoirs above the EWOD chip, unlike aqueous liquids. 20 µL liquid is pipetted between fluoropolymer coated slides that mimic the traditional EWOD chip geometry. The liquid-vapor surface tension (γ_{lv}) is tangential to the liquid-vapor interface. (a,b) For non-wetting liquids having contact angle θ>90^o the net surface tension force (F_γ) pushes liquid out from the gap. (c,d) Wetting liquids, e.g. organic solvents, having θ<90^o, are conversely pulled into the gap (outlined), which could lead to flooding if connected to a large reservoir.

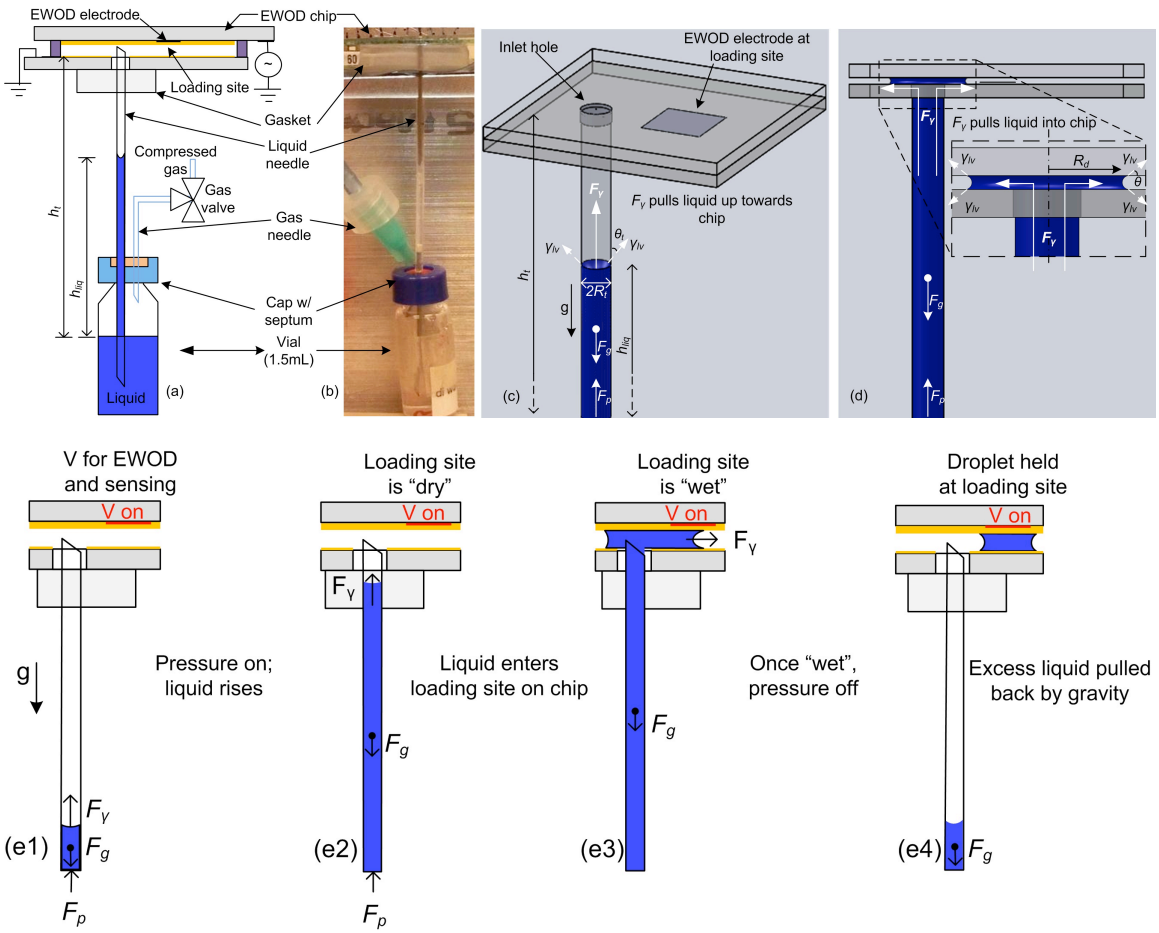

Fig. 2: (a) Schematic and (b) image of the setup to demonstrate the concept of pneumatic loading against gravity. (c) Forces acting on the liquid as it is rising in the tubing (assuming contact angle θ_t <90^o in the tubing).(d) Forces acting on the liquid as it is spreading in the chip (assuming contact angle θ <90^o in the chip). Note that the weight of the liquid within the chip is counter-balanced by the normal reaction, and therefore neither is shown. (e) Steps of operation: (e1-e2) The vial is pressurized so that F_p pushes the liquid up towards and into the chip. (e3) Liquid is sensed at the loading site, triggering the removal of F_p, and (e4) allowing gravity to retract the excess liquid, while the desired volume is retained by EWOD at the loading site.

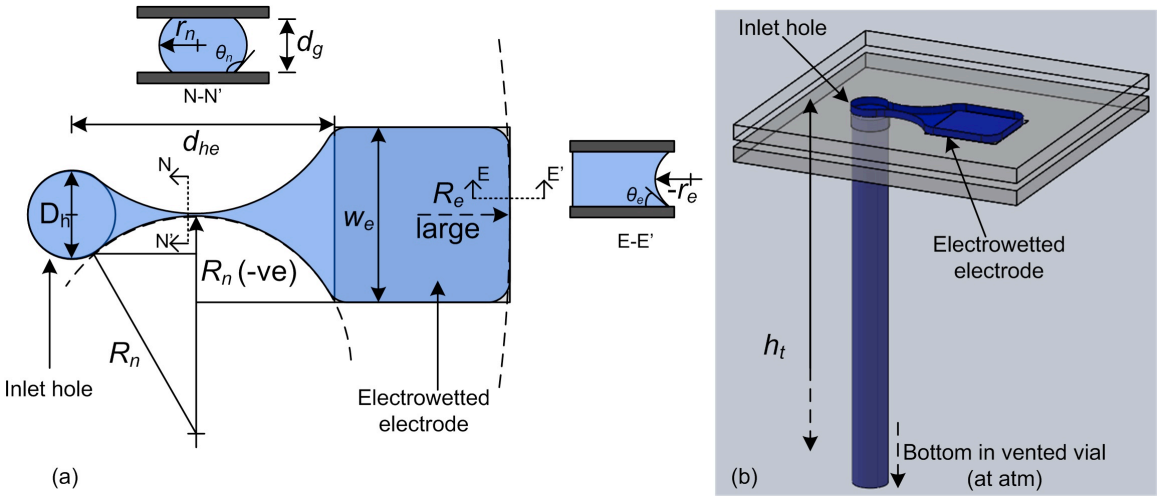

Figure 3: Relevant geometry to derive splitting criterion for gravity-driven droplet loading. (a) Top view, with cross-sectional views of the neck region (N-N') and EWOD electrode edge (E-E'). The cross-sectional view N-N' is shown for the case of a non-wetting liquid (θ_n>90^o); for a wetting liquid, θ_n would be <90^o. It is assumed that all liquids of interest wet the activated electrode as shown in the cross-section E-E'. (b) Isometric view of the necked droplet between inlet hole and the electrowetted EWOD electrode. Based on the geometry in the top view and cross-sectional views at the electrode edge (e) and the neck (n) regions, the principal radii of curvature at the two sites (r_n, r_e, R_n, R_e) can be determined. The two cross-sectional radii r_n and r_e are shown in the respective cross-sectional views. Using inlet hole radius, R_h, distance between the inlet hole and electrode, d_{he}, and the electrode width, w_e, the radius of curvature, R_n can be determined geometrically. Considering that the rightmost edge of the droplet conforms to the straight edge of the EWOD electrode, R_e is large.

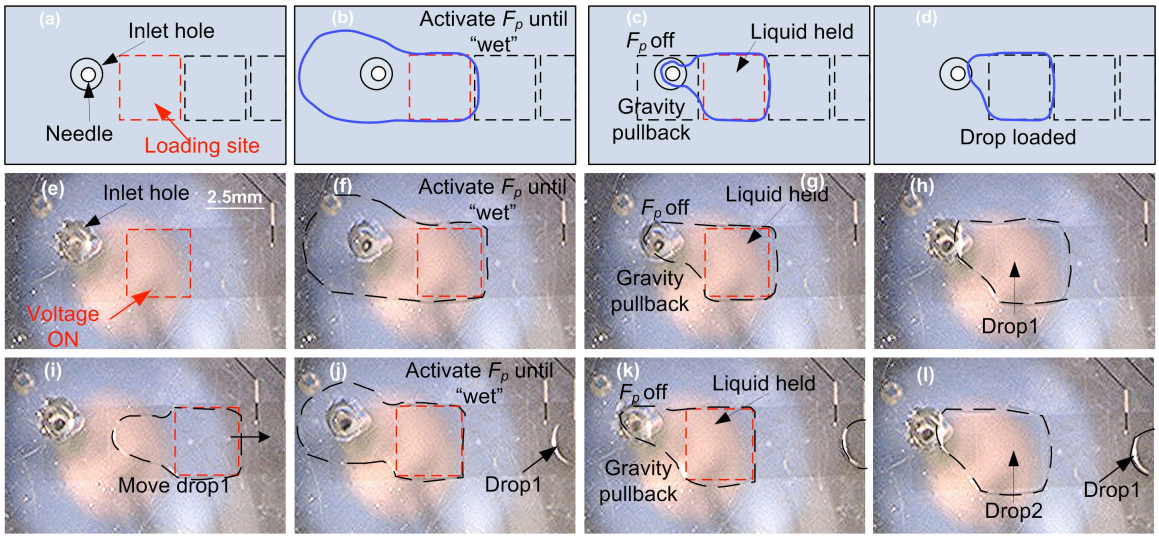

Fig. 4: On-demand loading of MeCN. (a-d) Schematic of EWOD electrodes and loading process. (e-h, i-l) Image sequence for loading of two successive droplets: (a,e) Upon demand for loading a droplet, voltage is turned on at the loading site (dashed red outline). (b,f,j) As pressure is applied, liquid rises and enters the chip from inlet hole. Though it initially spreads in all directions, the liquid preferentially wets the electrowetted loading site. (c,g,k) Once liquid is sensed ("wet"), pressure is turned off. Liquid at the loading site is retained by EWOD force, while the rest of the liquid is pulled back out of the chip by gravity. (d,h,l) Liquid splits between inlet hole and loading site to form a droplet. (i) Droplet is moved away, leaving the loading site "dry" until the next on-demand loading (shown in j, k, l). Each loading operation from (a to d) takes <5s. Dashed black outlines are included to clarify positions of some portions of droplets.

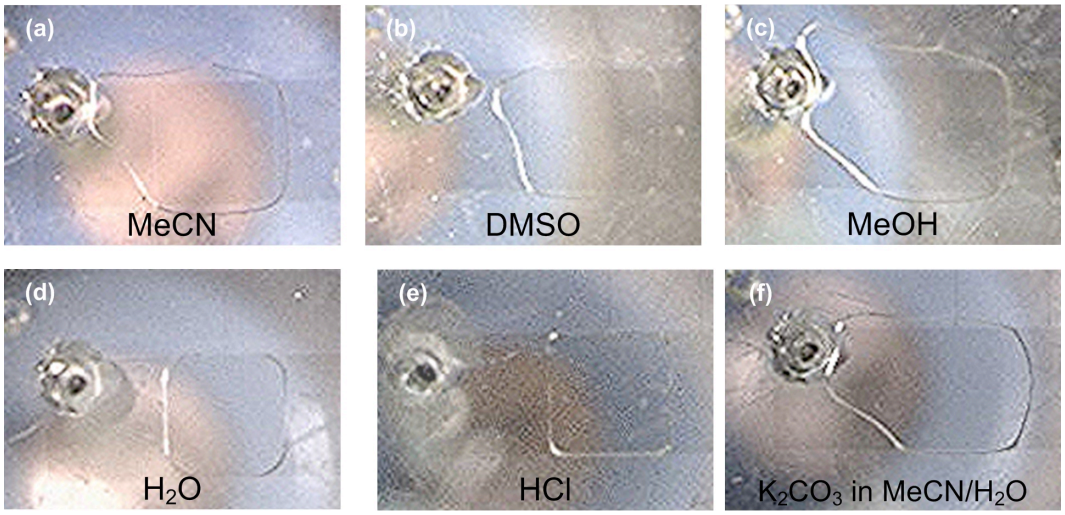

Fig. 5: Specimen images of droplets of various liquids loaded on-demand. (a-c) Common organic solvents- MeCN, DMSO and MeOH; (d) DI water; (e) 250mM HCl; (f) 20mM K_2CO_3 in a mixture of MeCN and water (95:5 v/v). While repeatability of size of consecutive droplets of the same liquid is high, there is a significant difference in size of droplets of different liquids.

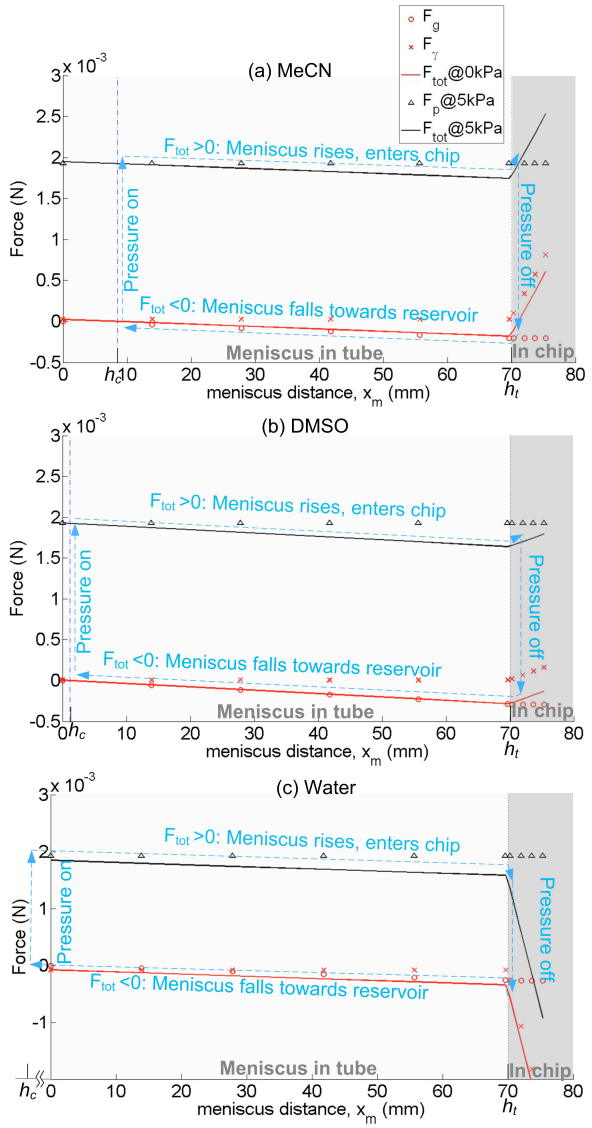

Fig. 6: Simulated forces on the meniscus vs. the position of the meniscus, x_m, as it rises up the tube (h_t=70mm) and then enters the chip, for three solvents: (a) MeCN, (b) DMSO and (c) water. When the meniscus is in the tube ($x_m \leq h_t$) with no pressure applied, the net force (solid red) determined by F_{grav} (-o- red) and F_γ (-x- red) keeps the meniscus at the capillary height, h_c. When pressure (e.g. 5kPa) is applied, the net force (solid black) is positive, raising the meniscus into the chip ($x_m > h_t$). Turning off the pressure switches from a positive to negative total force for all liquids, leading to deceleration and retraction of liquid towards the reservoir, preventing runaway flooding. The technique works for both wetting and non-wetting liquids.

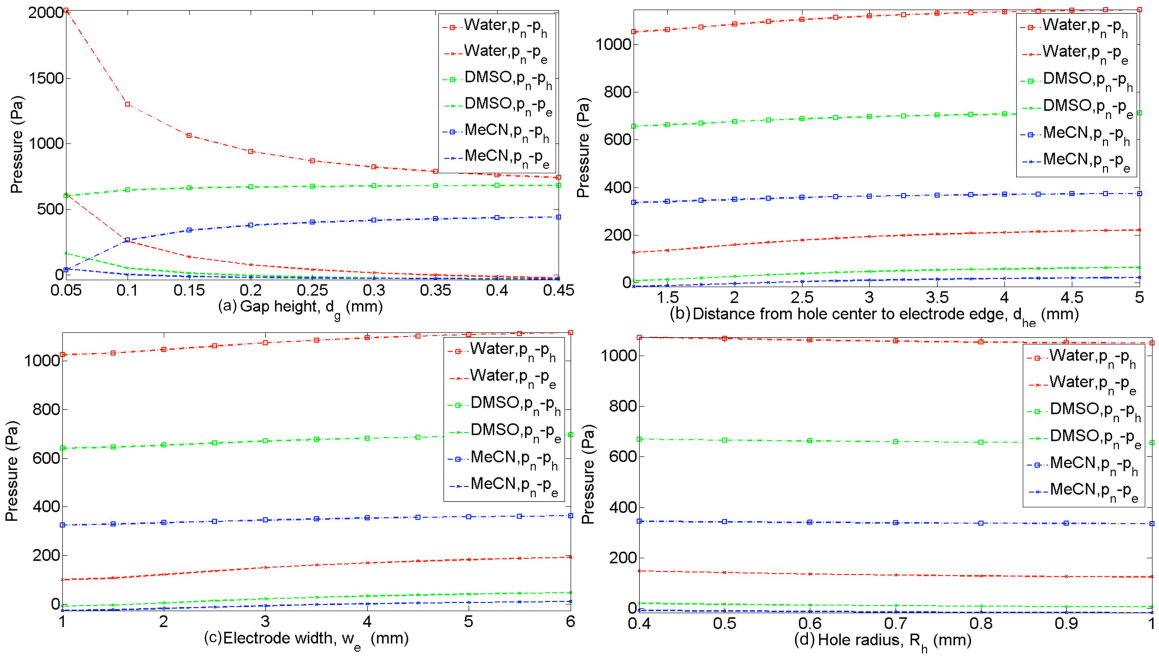

Fig. 7: Variation of splitting pressures (outward from the neck towards hole (p_n-p_h, -o- lines), and towards electrode (p_n-p_e, -- lines)) with various geometric parameters for three representative liquids- water (red), DMSO (green) and MeCN (blue). Overall, the greater magnitude of p_n-p_h as compared to p_n-p_e indicates that gravity provides an especially effective pullback force for a range of fluids. Additionally, the relatively greater magnitude of p_n-p_h and p_n-p_e for water, compared to the respective counterparts for MeCN and DMSO lead to quicker flow out of the necking region, perhaps suggesting why aqueous droplets dispensed to the chip are much more conformal to the EWOD electrode (Fig. 5).

Table 1: Theoretical capillary rise for aqueous and non-aqueous liquids in a tube with ID 0.6mm

Reagent	**Density (20^oC) (kg/m^3) [12]**	**Surface tension (mN/m) [10]**	**h_c (for θ_i=0) (mm)**	**Contact angle on Teflon (deg) [9]**	**h_c (Teflon) (mm)**
Water	1000	72	49	120	-24
DMSO	1100	43	27	87	1
Acetontrile	780	29	25	67	10

Table 2: Summary of on-demand loading of aqueous and non-aqueous droplets (n=5 each)

Reagent	**Volume (µL)**	**Standard Deviation (µL)**	**Standard Deviation (%)**
Water (H_2O)	0.840	0.017	2.0
Hydrochloric acid (HCl)	0.903	0.013	1.4
Dimethyl sulfoxide (DMSO)	1.086	0.030	2.8
Methanol (MeOH)	1.652	0.063	3.8
Acetontrile (MeCN)	1.442	0.073	5.1
K_2CO_3 in MeCN/H_2O	1.445	0.057	3.9